

Exact Study of the 1D Boson Hubbard Model with a Superlattice Potential

V.G. Rousseau,¹ D.P. Arovas,² M. Rigol,¹ F. Hébert,³ G.G. Batrouni,³ and R.T. Scalettar¹

¹*Physics Department, University of California, Davis, California 95616, USA*

²*Physics Department, University of California, San Diego, California 92093, USA*

³*Institut Non Linéaire de Nice, 1361 route des Lucioles, 06560 Valbonne, France*

We use Quantum Monte Carlo simulations and exact diagonalization to explore the phase diagram of the Bose-Hubbard model with an additional superlattice potential. We first analyze the properties of superfluid and insulating phases present in the hard-core limit where an exact analytic treatment is possible via the Jordan-Wigner transformation. The extension to finite on-site interaction is achieved by means of quantum Monte Carlo simulations. We determine insulator/superfluid phase diagrams as functions of the on-site repulsive interaction, superlattice potential strength, and filling, finding that insulators with fractional occupation numbers, which are present in the hard-core case, extend deep into the soft-core region. Furthermore, at integer fillings, we find that the competition between the on-site repulsion and the superlattice potential can produce a phase transition between a Mott insulator and a charge density wave insulator, with an intermediate superfluid phase. Our results are relevant to the behavior of ultracold atoms in optical superlattices which are beginning to be studied experimentally.

PACS numbers: 05.30.Jp, 71.10.Fd, 02.70.Uu

I. INTRODUCTION

Originally proposed as a model for short-coherence length superconductors and Josephson junction arrays, the boson Hubbard Hamiltonian¹ has over the last several years been widely used to understand the physics of ultra-cold optically-trapped atoms.² While previous work had considered translationally invariant systems^{3,4,5,6,7,8} or the effect of a random chemical potential in order to understand glassy behavior,^{9,10} a key feature of the model as applied to cold atoms is the inclusion of a (usually quadratic) external potential which reflects the magnetic confinement. This potential leads to a number of interesting effects including the coexistence of superfluid and Mott insulating regions within the trap.^{2,11,12}

Early on in the application of the Bose-Hubbard model to optically confined atoms, the study of a “superlattice” in which the confining potential has multiple minima was considered.² Upon increasing the chemical potential, the density profile evolves from a situation where the boson densities in the different minima are independent to one where superfluid ‘necks’ develop and join the bosons in the different minima. Subsequently, further mean field theory treatments developed a more quantitative understanding of the phase diagram, in the case when the superlattice potential varies with a period of $T = 2, 3$ and 4 sites.^{13,14,15} Mott insulating phases with fractional fillings exist, and, interestingly, under certain circumstances the usual Mott phase at $\rho = 1$ can be absent. The physics of the Bose-Hubbard Hamiltonian with aperiodic potentials,^{16,17} in which localization without disorder can occur, has also been discussed.¹⁸

Various experimental realizations of such multiple well superlattices have been proposed, from a double well magnetic trap for Bose-Einstein condensations in which the barrier height and well separation are smoothly controllable,¹⁹ to periodic potentials where the lattice

constant is especially large, allowing the loading of many bosons per minimum.^{20,21} Superlattice potentials similar to the ones considered in this work have been realized by Peil *et al.*²² One of the great advantages of these ultracold gas realizations of strongly correlated systems is the experimental possibility to tune all parameters at will.

In this paper we use Quantum Monte Carlo (QMC) simulations and exact diagonalization to study the physics of the boson Hubbard Hamiltonian and its infinite U limit in the presence of a superlattice potential. In contrast to previous mean-field studies,^{13,14,15} we consider the hopping parameter to be independent of the position in the lattice. In addition, our numerical approaches provide an exact treatment of correlations that are particularly important in one dimension. We also compute important quantities like the superfluid density and the momentum distribution function, which make connections with experiments. Superlattice potentials similar to the ones considered in this work have been realized by Peil *et al.*²² and Sebby-Strabley *et al.*³⁰ One of our main results is that the superlattice produces insulating phases for commensurate fractional fillings. For the hard-core case, this behavior can be explained in terms of band structures by performing an exact mapping onto a spinless fermionic system. Insulating behavior persists for the soft-core case with sufficient on-site repulsion. On the other hand, at integer fillings, changing the ratio between the on-site repulsion and the strength of the additional superlattice potential can produce an intermediate superfluid phase between Mott insulating and charge density wave phases.

The exposition is organized as follows. In Sec. II, we study the infinite U limit of the boson Hubbard Hamiltonian with an additional superlattice potential. The generalization to finite on-site interactions is presented in Sec. III, where we use QMC simulations to solve the problem exactly. We also present in Sec. III an analy-

sis of the atomic limit that helps to understand results for large but finite U , where multiple occupancy of the lattice sites is allowed. In Sec. IV, we present a theoretical analysis extending the atomic limit by allowing finite hopping amplitudes, which gives further insight on our numerical results for large values of U . Finally, the conclusions are presented in Sec. V.

The translationally invariant boson Hubbard model¹ is:

$$\hat{\mathcal{H}} = -t \sum_{\langle ij \rangle} (a_i^\dagger a_j + a_j^\dagger a_i) + U \sum_i \hat{n}_i (\hat{n}_i - 1) \quad (1)$$

The operators a_i^\dagger, a_i create (destroy) a boson on site i , and obey commutation rules $[a_i, a_j^\dagger] = \delta_{ij}$. The number operator is $\hat{n}_i = a_i^\dagger a_i$. The hopping parameter t measures the kinetic energy and U the strength of the on-site repulsion. We will consider a one dimensional lattice so that the sum $\langle ij \rangle$ over near neighbors has $j = i + 1$. The ground state phase diagram is well known.^{1,3,4,5,6,7,8} At commensurate fillings, and for sufficiently large U , the bosons are in a gapped Mott insulating phase. Away from integer filling, or for weak coupling, the system is superfluid. In the limit $U \rightarrow \infty$ this model maps onto the spin 1/2 XY model, with the z component of magnetization playing the role of the boson density.

To obtain a superlattice, we consider a case where a low amplitude, long wavelength potential is added to the usual high intensity short wavelength optical potential which generates the lattice in which the atoms move. (See Fig. 1). Atoms in the resulting superlattice thus have a hopping parameter which is independent of spatial position. This is completely analogous to the usual optical trap configuration and associated model calculations. The long period potential we consider has the form

$$V_{\text{ext}} = A \sum_j \cos \frac{2\pi j}{T} \hat{n}_j. \quad (2)$$

We will be interested in understanding the ground state phase diagram as a function of the energy scales $U/t, A/t$, particle density ρ , and the period T .

II. ANALYTIC TREATMENT OF THE HARD-CORE LIMIT

We first consider the hard core limit, $U = \infty$, which is exactly solvable via the Jordan-Wigner transformation,

$$a_j^\dagger = c_j^\dagger \prod_{n=1}^{j-1} e^{i\pi c_n^\dagger c_n}. \quad (3)$$

If the boson operators obey general twisted boundary conditions $a_{L+1}^\dagger = e^{-i\delta} a_1^\dagger$, it proves convenient to invoke

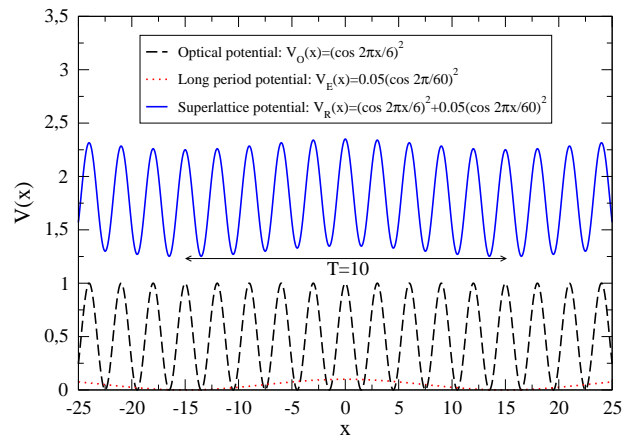


FIG. 1: (Color online) An example of a superlattice potential we study in this work. The long period potential provides a small additional modulation to the deep optical potential which produces the lattice. As a consequence, the hopping parameter t is independent of position.

a unitary transformation to transfer the boundary condition phase from the bosonic operators to the hopping integrals, *viz.*

$$\hat{\mathcal{H}} = - \sum_{n=1}^L (t'_{n,n+1} a_n^\dagger a_{n+1} + \text{H.c.}) + A \sum_{n=1}^L \cos \left(\frac{2\pi n}{T} \right) a_n^\dagger a_n, \quad (4)$$

where $a_{L+1}^\dagger = a_1^\dagger$ and $t'_{n,n+1} = t$ for $1 \leq n < L$ and $t'_{L,1} = e^{i\delta} t$. When mapping this Hamiltonian, with the additional on-site hard-core constraints

$$a_n^{\dagger 2} = a_n^2 = 0, \quad \{a_n, a_n^\dagger\} = 1, \quad (5)$$

onto a non-interacting fermionic Hamiltonian one notices that

$$a_1^\dagger a_L = -c_1^\dagger c_L \prod_{n=1}^L e^{i\pi c_n^\dagger c_n}, \quad (6)$$

which means that the equivalent fermionic Hamiltonian takes the form

$$\hat{\mathcal{H}} = - \sum_{n=1}^L (t_{n,n+1} c_n^\dagger c_{n+1} + \text{H.c.}) + A \sum_{n=1}^L \cos \left(\frac{2\pi n}{T} \right) c_n^\dagger c_n, \quad (7)$$

where $c_{L+1}^\dagger = c_1^\dagger$ and $t_{n,n+1} = t$ for $1 \leq n < L$ and $t_{L,1} = e^{i(\delta+\eta)} t$, depending on whether $N = \langle \sum_{n=1}^L c_n^\dagger c_n \rangle$ is even ($\eta = \pi$) or odd ($\eta = 0$). Via a second unitary transformation, we can impose the boundary phase uniformly over the hopping integrals, yielding $t_{n,n+1} = e^{i(\delta+\eta)/L} t$ for all n .

We now transform to a quasi-momentum basis, writing $c_n^\dagger = L^{-1/2} \sum_k e^{-ikn} c_k^\dagger$, where k is quantized with $e^{ikL} = 1$. The superlattice potential couples states of quasi-momenta k and $k \pm Q$, where $Q = 2\pi/T$. Restricting k to the reduced Brillouin zone (BZ) $[-\frac{\pi}{T}, \frac{\pi}{T}]$, the

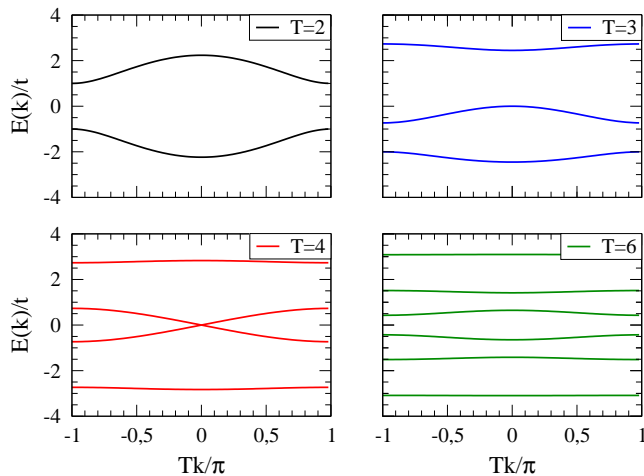


FIG. 2: (Color online) Band structure of the hard-core Bose Hubbard model for periods $T = 2, 3, 4, 6$. The two central energy bands in the $T = 4$ case touch, and the system is not an insulator at $\rho = \frac{1}{2}$.

matrix elements of $\hat{\mathcal{H}}$ are

$$\begin{aligned} \mathcal{H}_{l,l'}^k &= \langle k + lQ | \hat{\mathcal{H}} | k + l'Q \rangle \\ &= -2t \cos(k + \zeta + lQ) \delta_{l,l'}^T + \frac{1}{2} A \delta_{|l-l'|,1}^T, \end{aligned} \quad (8)$$

where $\zeta = (\delta + \eta)/L$, and $\delta_{l,l'}^T = \delta_{l,l' \bmod T}$. This defines a $T \times T$ matrix for each k in the reduced zone. The eigenvalues give the T energy bands $E_\alpha(k)$. The $T = 2$ case is familiar:

$$E_\pm(k) = \pm \sqrt{4t^2 \cos^2(k + \zeta) + A^2} \quad (9)$$

The effect of the periodic potential is to open up gaps at the boundaries of the reduced BZ. Figure 2 shows the band structure for $T = 2, 3, 4, 6$. There are energy gaps at $\rho = \frac{1}{2}$ for $T = 2$, at $\frac{1}{3}$ and $\frac{2}{3}$ for $T = 3$, at $\rho = \frac{1}{6}, \frac{2}{6}, \frac{3}{6}, \frac{4}{6}, \frac{5}{6}$ for $T = 6$. However, for $T = 4$ the energy bands cross at $\rho = \frac{1}{2}$ and gaps exist only at $\frac{1}{4}$ and $\frac{3}{4}$.

Taking $t/A \rightarrow 0$ yields the atomic limit. For $t = 0$, the energy levels are $E_n^0 = A \cos(2\pi n/T)$. For small t/A , the bandwidth of each of the T bands may be obtained to leading order by appealing to the locator expansion for the Green's function, as we show in Appendix A.

Because the number of bands is equal to the number of sites per supercell, one expects that the system is insulating at half filling when the period T is an even number. For such cases the first $T/2$ bands are completely filled, and the creation of an exciton requires a finite supply of energy. However it can happen that the valence band crosses the conduction band, as illustrated in Fig. 2 for $T = 4$. Then no gap arises, and the system is not insulating. As shown in Appendix A, this situation occurs (for $\rho = \frac{1}{2}$) whenever $T = 4p$, p being an integer. The situation is depicted in Fig. 3. For $T = 4p + 2$ a gap occurs, and decays as a power law as a function of T for a fixed value of A . (This is shown in the inset, where a

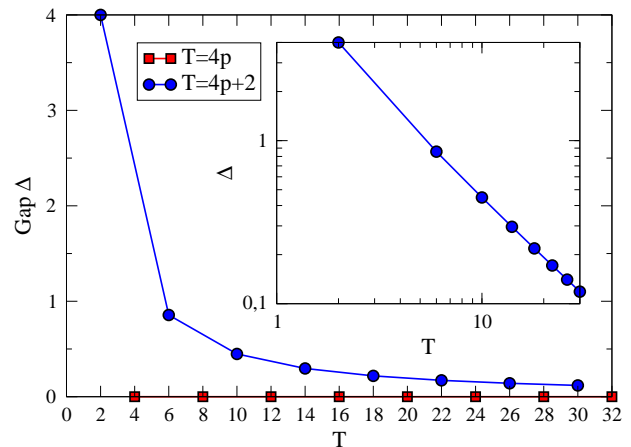


FIG. 3: (Color online) The gap Δ as a function of T for $t = 1$ and $A = 2$ at half filling. Δ is finite only for $T = 4p + 2$. The inset shows the same plot but with logarithmic axes, emphasizing a power law decay which is discussed in the text.

fit provides an exponent of -1.03 for $A/t = 2$). In the atomic limit, we have $\Delta = 2A \sin(\frac{\pi}{T})$, hence $\Delta \propto T^{-1}$ at large T . For odd values of T , the system at half-filling is never insulating because the highest occupied band is itself half-filled.

The dimensionless superfluid density is given by the expression

$$\rho_s = \left. \frac{L}{2t} \frac{\partial^2 F}{\partial \delta^2} \right|_{\delta=0} \quad (10)$$

$$= \frac{\hbar v_F}{2\pi t} \quad (\Theta = 0, L = \infty), \quad (11)$$

where F is the free energy and $v_F = \frac{1}{\hbar} \frac{\partial \varepsilon_n}{\partial k|_{k_F}}$ is the Fermi velocity. The second expression, valid at temperature $\Theta = 0$ in the thermodynamic limit $L = \infty$, follows from the fact that $\partial E_n / \partial \delta = L^{-1} \partial E_n / \partial k$. We see from this last expression that the superfluid density vanishes whenever the Fermi level lies within a band gap. Furthermore, if the last partially occupied fermion band is nearly filled or nearly empty, then $v_F \approx \hbar k_F / m^*$, with the effective mass $(m^*)^{-1} = \frac{1}{\hbar^2} \frac{\partial^2 \varepsilon_n}{\partial k^2}$, and the dimensionless density is $\rho = \rho_{\text{Mott}} + \delta\rho$, with $\delta\rho = \pm k_F / \pi$. Therefore we find

$$\rho_s(\rho) = \frac{m}{m^*} |\rho - \rho_{\text{Mott}}|, \quad (12)$$

where $m \equiv \hbar^2 / 2ta^2$ is the bare ‘mass’ (a being the physical lattice constant), and ρ_{Mott} is the density corresponding to an integer number of filled bands.

Another definition of superfluid density, which becomes exact in the thermodynamic limit, is based on the free energy difference between periodic ($\delta = 0$) and antiperiodic ($\delta = \pi$) boundary conditions:

$$\rho_s = \lim_{L \rightarrow \infty} \rho_s^L \quad \rho_s^L = \frac{L(F_\pi - F_0)}{t\pi^2}, \quad (13)$$

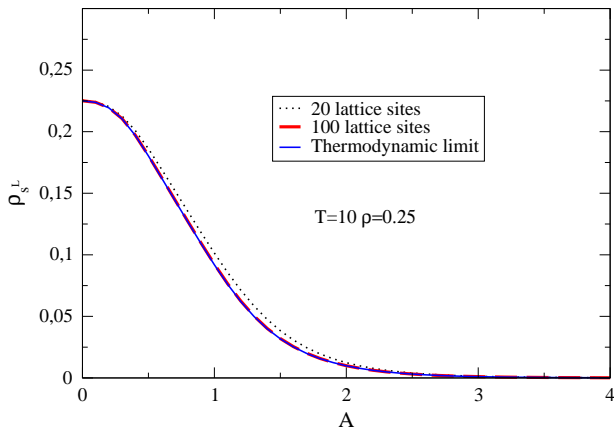


FIG. 4: (Color online) The superfluid density, ρ_s , with $\rho = 0.25$ and $T = 10$ as a function of A . We show results for two values of the system size L , and the thermodynamic limit result Eq. (11). No difference is perceptible between the results for $L = 100$ and $L = \infty$.

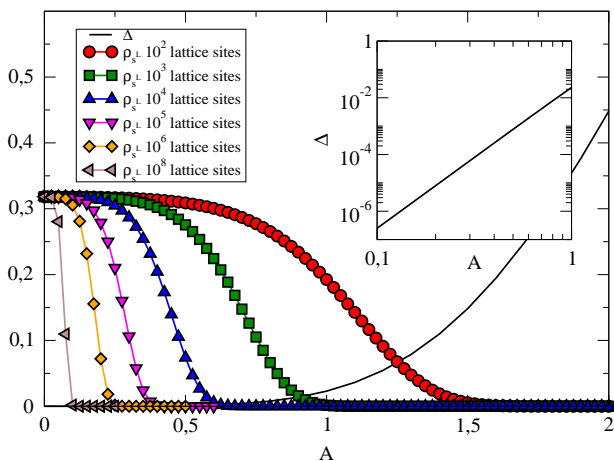


FIG. 5: (Color online) ρ_s^L and gap Δ for $T = 10$ at half filling, as functions of A . For this filling, the critical value of A for which ρ_s^L vanishes shows a tendency to go to zero, when increasing the size of the system. This is due to the gap Δ which vanishes only at $A = 0$. For small but finite A , Δ follows a power law with the exponent 4.97.

where F_δ is the free energy at boundary phase δ . Eq. (13) is of course equivalent to a discrete approximation to the second derivative in Eq. (10), but it has the advantage of being easier to evaluate numerically. We find that in the superfluid phases finite size effects related to the definition in Eq. (13) start to be negligible for quite small system sizes, of the order of $L \approx 100$. This is shown in Fig. 4 which displays the values of the superfluid density, ρ_s , for $\rho = 0.25$, $T = 10$ as a function of A obtained for two finite systems ($L = 20, 100$) following Eq. (13) and the thermodynamic limit calculation following Eq. (11). The curve for $L = 100$ is perfectly superposed to the thermodynamic limit result, and even $L = 20$ gives a very good estimation of ρ_s .

We should stress, however, that in the insulating phases, i.e., for commensurate fillings where ρ_s is zero, finite size effects become relevant in Eq. (13) when the gap approaches zero as A decreases. For those cases one needs to take the limit $L \rightarrow \infty$ to obtain the correct $\rho_s = 0$. This can be seen in Fig. 5 where ρ_s^L [Eq. (13)], and the gap Δ , are plotted as functions of the amplitude A of the modulating potential, for $T = 10$, half filling, and different values of L . The inset shows the gap with logarithmic axes, emphasizing a decay with a power law when A goes to zero, with an exponent of 4.97, consistent with the exact value of 5 obtained from locator expansion of the Green's function for the Hamiltonian in Eq. (8).

From the viewpoint of the fermion Hamiltonian, we might regard the insulating phases at fractional densities corresponding to complete filling of each $E_n(k)$ as ‘band insulators’. However, when the hard core constraint is lifted, the insulating phases of the bosons are more properly regarded as ‘Mott insulators’. Consider, for example, the $T = 2$ case. The eigenvectors of the lowest energy band $E_-(k)$ have their largest density on those spatial sites with superlattice potential $-A$. If U is sufficiently weak, multiple occupancy of this spatial sublattice will not be energetically forbidden, and there is no reason to expect then an insulating phase at $\rho = \frac{1}{2}$. Thus, as U is decreased, one eventually will reach a quantum critical point where the gap vanishes and the system becomes superfluid. This is indeed what emerges from our Quantum Monte Carlo analysis of the soft-core model, discussed further below.

In Fig. 6, we plot the superfluid density ρ_s and energy gap Δ for the $T = 10$ system *versus* the filling ρ . As expected, Δ is finite only for $\rho = j/T$, where an integer j number of bands are completely filled. The superfluid density ρ_s exhibits local maxima at $\rho = (j + \frac{1}{2})/T$, in the centers of the bands. We note that ρ_s is greatest in the central bands, and smallest in the outer bands. Indeed, the superfluid density must be small when ρ itself

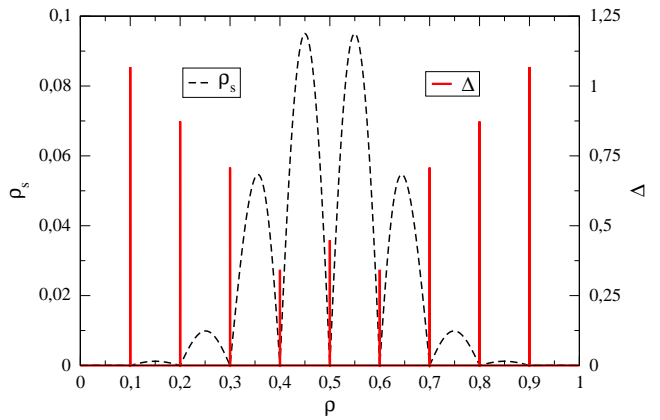


FIG. 6: (Color online) Superfluid density ρ_s and gap Δ of the hard-core boson Hubbard Hamiltonian for $T = 10$, $t = 1$, and $A = 2$. Gapped band insulating phases exist at fillings $\rho = \frac{1}{10}, \frac{2}{10}, \frac{3}{10}, \dots$

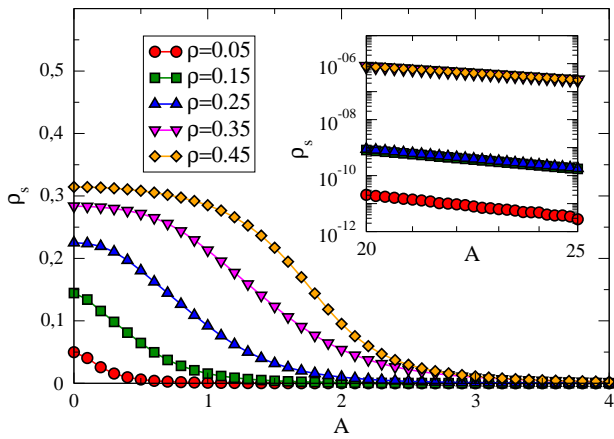


FIG. 7: (Color online) Superfluid density ρ_s for $T = 10$ and different fillings, as functions of A , with $t = 1$. ρ_s decays as a power law (see text for the exponents).

is small, since there are fewer bosons to contribute to ρ_s . As ρ increases (restricting our attention to the band centers), ρ_s increases concomitantly, until one passes $\rho = \frac{1}{2}$, when the trend reverses. For large ρ one should think in terms of superfluidity of *holes* (*i.e.* empty sites).

Figure 7 shows ρ_s for several fillings as functions of A , for $T = 10$. The inset corresponds to the same plot but with logarithmic axes, showing a power law decay of ρ_s . The numerically extracted exponents are -8.47 for $\rho = 0.05$, -6.94 for $\rho = 0.15$, -7.06 for $\rho = 0.25$, and -5.00 for $\rho = 0.35$ and $\rho = 0.45$. These values compare well with the exact results for m^* derived earlier from the locator expansion: $(m^*)^{-1} \propto t^T/A^{T-1}$ for bands arising from atomic levels $E_n^0 = A \cos(\frac{2\pi n}{T})$ which are nondegenerate ($n = 5$ for $\rho = 0.05$), and $(m^*)^{-1} \propto t^{2n}/A^{2n-1}$ arising from degenerate atomic levels ($n = 4$ for $\rho = 0.15$ and $\rho = 0.25$; $n = 3$ for $\rho = 0.35$ and $\rho = 0.45$).

The full phase diagram for $T = 10$ is shown in Fig. 8. The gapped insulating phases extend all the way down to $A = 0$, as there is a finite gap for any finite value of A (Fig. 5). As A/t increases, off the magic densities, ρ_s goes to zero as a power law (Fig. 7), and for this reason the associated regions of the phase diagram (red color) are labeled 'weakly superfluid'.

To conclude this section we discuss how the superfluid and Mott insulating phases introduced above could be detected in experiments with ultracold bosons on optical lattices. For that we study the imprint of these phases in the hard-core boson momentum distribution function $[n(k)]$,²³ which is a quantity that can be easily obtained in time of flight measurements.

Figure 9 shows $n(k)$ for $T = 10$, $\rho = 0.45$ (superfluid case), and three values of A . For $A = 0$ (top panel), a single peak can be seen at $n(k = 0)$ with a height that scales proportional to the square root of the number N of particles in the system, and thus diverges in the thermodynamic limit.²³ This peak signals quasi-long range one-particle correlations typical of the superfluid state in

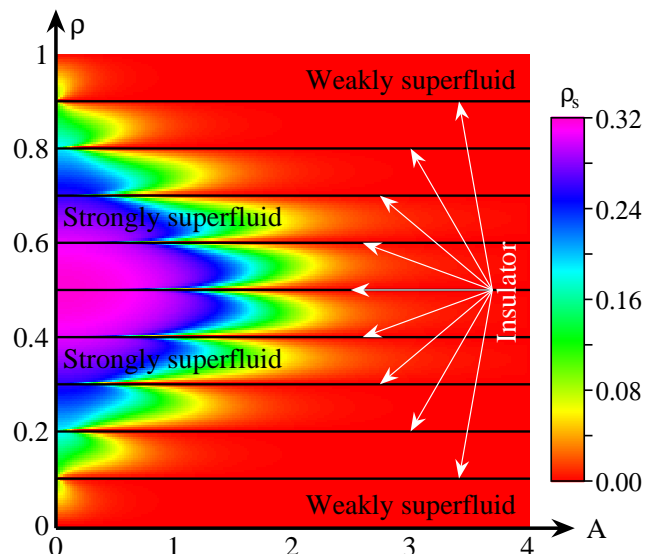


FIG. 8: (Color online) Phase diagram of the hard-core Bose Hubbard model as a function of filling ρ and strength A of the superlattice potential. Fillings $\rho = \frac{1}{10}, \frac{2}{10}, \frac{3}{10}, \dots$ are insulating for all $A \neq 0$. At fillings which are not commensurate with the superlattice potential, the superfluidity becomes small at large A . (See Figure 7).

1D. The introduction of the additional potential in Eq. (2) introduces a modulation in the one-particle correlations but does not destroy their quasi-long range order. As a consequence one can see in the two lowest panels of Fig. 9 that additional sharp peaks appear with momenta $k = \pm \frac{n\pi}{10}$.

On the other hand, in the insulating phases (at commensurate fillings) the opening of a gap in the one particle excitation spectrum produces an exponential decay of the one-particle correlations. As seen in Fig. 10, this exponential decay destroys the sharp peaks observed at $n(k = 0)$ in the superfluid state (top panel). As a consequence, a very broad distribution is observed in $n(k)$ with no additional satellite peaks at $k = \pm \frac{n\pi}{10}$ (two lowest panels). Hence, measuring $n(k)$ in experiments would unambiguously differentiate between the superfluid and insulating phases we have analyzed in this section.

III. QUANTUM MONTE CARLO SIMULATIONS OF THE SOFT-CORE CASE

As a first step in studying the soft-core case, it is worthwhile to recall the phase diagram of the uniform case $A = 0$ in the $(\mu/U, t/U)$ plane (Fig. 11). In this situation the system is superfluid, except for integer densities and sufficiently large on-site repulsion. In this latter case, we have an incompressible Mott insulator. The transitions between superfluid and Mott insulating phases in the d -dimensional boson Hubbard model are known to be mean field like when driven by a change of the density, and of

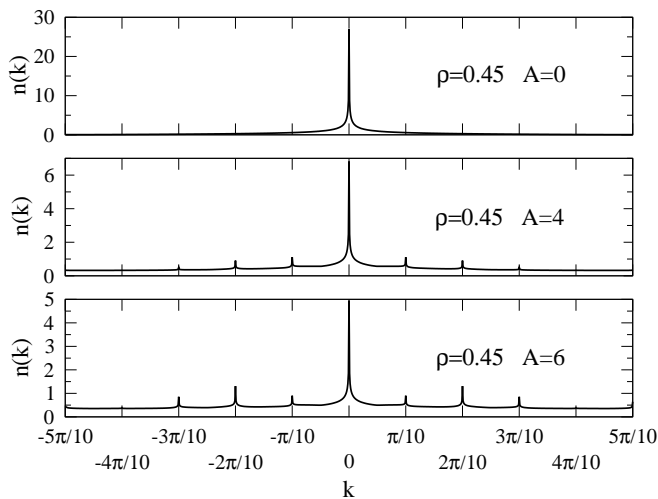


FIG. 9: The momentum distribution function for $\rho = 0.45$. Top panel: The superlattice is turned off, and we have a quasi-condensate in the zero momentum state. Middle and bottom panels: As A is turned on, some particles leave the zero momentum state and go into higher momentum states. New peaks emerge at those momenta commensurate with the superlattice. These sharp peaks signal that the system is in a (gapless) superfluid state even if the superfluid density is very small (Fig. 8).

the $(d+1)$ dimensional XY universality class when at integer densities the transition is driven by changing the on-site repulsion U .^{1,3,4,5,6,7,8}. In particular, in 1D the

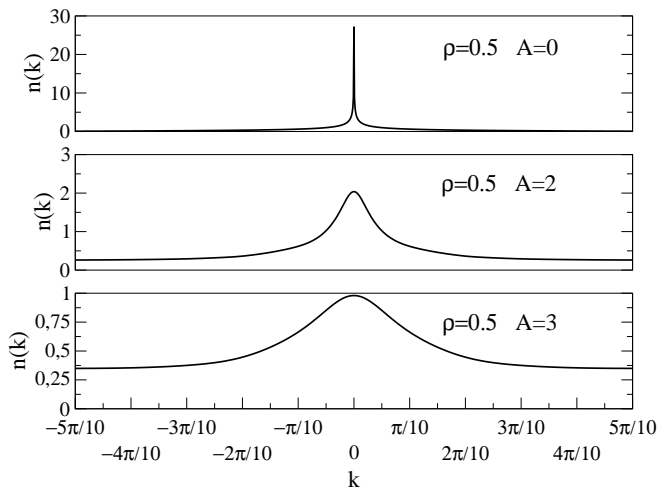


FIG. 10: The momentum distribution function for $\rho = 0.5$. Top panel: For $A = 0$, there is no superlattice potential and the distribution looks similar to Fig. 9, corresponding to a quasi-condensate. Middle and bottom panels: For $A = 2$ and $A = 3$, the density is commensurate with the superlattice leading to an insulating state. The momentum distribution very broad due to the absence of quasi-condensation. No additional peaks are observed at momenta commensurate with the superlattice. These two features signal the presence of a (gapped) insulating state.

Mott region with $\rho = 1$ starts to develop at $U \approx 2$ and for $\rho = 2$ starts at $U \approx 4$.^{3,4,5,6,7,8}

A. Atomic limit

Before discussing the general case, $t \neq 0$, $U \neq 0$, and $A \neq 0$, a useful step is to consider first the atomic limit $t = 0$. In this case the Hamiltonian is diagonal in the occupation number basis, and the ground state is obtained by filling the system in a way which minimizes the energy, depending on the competition between U and A . The on-site repulsion on one hand tends to avoid multiple occupancies, leading to Mott insulators at integer densities. On the other hand, the modulating potential tends to trap the particles into its minima, leading to a density profile which reflects the modulation. In particular, for $T = 2$, the modulating potential tends to impose a charge density wave (CDW) which results in alternatively highly and weakly occupied sites.

For a given on-site repulsion U , we start to fill the system from $\rho = 0$ by putting the particles alone on low energy sites until $\rho = \frac{1}{2}$. Each time a particle is added, the energy decreases by steps of $-A$, resulting in a chemical potential $\mu = -A$. Adding more particles leads to a competition between U and A . If $A < U$, the energy is minimized by putting the new particles on high energy sites, increasing the total energy by steps of A . On the contrary, if $A > U$, the on-site repulsion will not avoid double occupancies and the energy will increase by steps of $2U - A$. As a result the value of the chemical potential from $\rho = \frac{1}{2}$ to $\rho = 1$ will be $\mu = \min(A, 2U - A)$.

Considering all possibilities of filling the system allows us to draw the phase diagram of the atomic limit in the $(\mu/U, A/U)$ plane (Fig. 12). Regions labeled as “Mott” refer to configurations where the density ρ is integer with a uniform profile. The structure factor

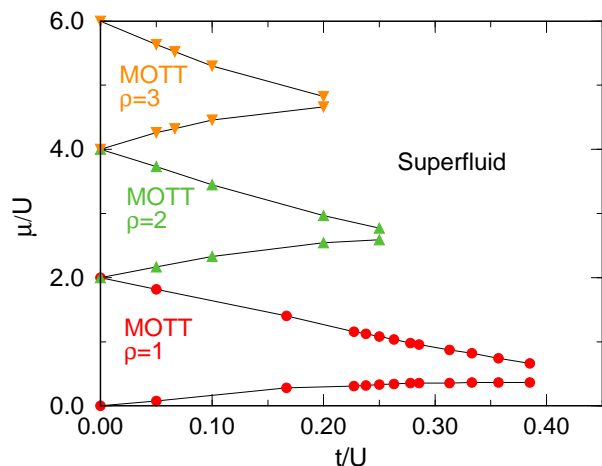


FIG. 11: (Color online) The phase diagram of soft-core bosons in the uniform case $A = 0$.

$S(k) = (1/L^2) \sum_{jj'} \langle \hat{n}_j \hat{n}_{j'} \rangle e^{-ik(j-j')}$ then presents only one peak in $k = 0$ with $S(0) = \rho^2$. Regions with label “CDW n ” refer to staggered phases where the difference between the density on low energy sites and high energy sites is n . Phases CDW n with n even occur for integer densities, and phases with n odd for half-integer densities. They have a signature in the structure factor which results in the development of a peak for $k = \pi$, with $S(\pi) = \frac{n^2}{4}$.

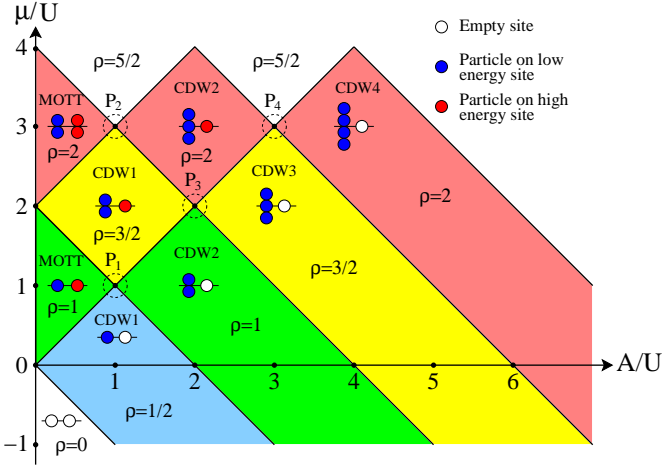


FIG. 12: (Color online) The phase diagram of soft-core bosons in the atomic limit $t = 0$ (see text for details).

B. General case

For our QMC computations, we used the World Line algorithm.^{24,25} When turning on the modulating potential, it is interesting to look first at the case with period $T = 2$. At finite, but large, on-site repulsion one can expect to obtain incompressible regions for the same fractional densities as the hard-core case. This is because a small $1/U$ acts like a perturbation to the noninteracting spinless fermion Hamiltonian,²⁶ i.e., it should not change the nature of the phases present for infinite U . Moreover, for low values of A and sufficiently large U , we can expect incompressible regions with $\rho = n$ (n being an integer), since this time it is A which acts as a perturbation on the translationally invariant boson Hubbard model (Eq. (1)). Figure 13 shows the density ρ as a function of the chemical potential μ for $T = 2$, $A = 2$, and different values of U . The slopes of these curves, $\frac{\partial \rho}{\partial \mu}$, are proportional to the isothermal compressibility. As a result, any discontinuity of μ (a gap) corresponds to a vanishing compressibility (presence of a plateau). Starting with $U = 1$, we can see that such a “band” discontinuity occurs for $\rho = \frac{1}{2}$, as expected. As we increase U , the gap at $\rho = \frac{1}{2}$ becomes larger and eventually a “Mott” gap opens at $\rho = 1$ as manifested by the plateau in Fig. 13. This corresponds to the first lobe in Fig. 11. Thus, the soft-core system

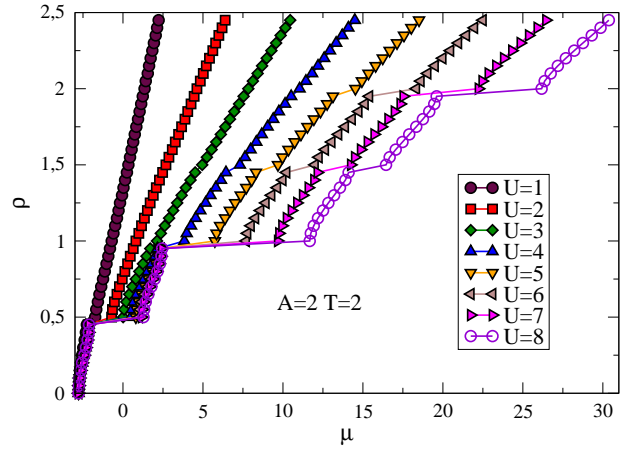


FIG. 13: (Color online) The density of particles as a function of the chemical potential for $T = 2$, $A = 2$, and different values of the on-site repulsion U .

is able to reproduce properties of the hard-core case (a gap at $\rho = \frac{1}{2}$), and properties of the uniform soft-core model (a gap at $\rho = 1$). In addition, a new gap for $\rho = \frac{3}{2}$ appears starting from $U = 3$. Increasing the on-site repulsion further leads to the presence of a gap at $\rho = 2$, corresponding to the second lobe of Fig. 11. Simulations show that gaps appear also for other integer and half integer densities ($\rho = \frac{5}{2}, \frac{6}{2}, \frac{7}{2}, \dots$) with strong on-site repulsion.

One can wonder how our QMC calculations are relevant to the zero temperature limit. Our algorithm determines the superfluid density by extrapolating to zero frequency the Fourier transform of the pseudo-current correlation function $\langle j(\tau)j(0) \rangle$.²⁴ This gives the mean square value of the winding number, which is related to ρ_s as defined by Eq. (10).²⁷ The advantage of computing ρ_s this way is that the measured value does not suffer from finite size effects (we have considered $L \geq 20$), and can give the value of ρ_s relevant to the zero temperature limit using an inverse temperature β not too large (we have taken $\beta \gtrsim 16$). This is shown in Fig. 14 which displays exact analytical and numerical results of ρ_s in the hard-core limit for $\Theta = 0$ and $L = \infty$, and QMC computations at finite temperature ($\beta = 16$), and finite system size ($L = 20$) as a function of the filling ρ . The data are in quite good agreement, and we can then expect this to hold in the soft-core case.

In Fig. 15 we show the superfluid density ρ_s in the soft-core case as a function of the density ρ for $A = 2$, and $T = 2$. It is to be compared with Fig. 13 and 14. Several things are apparent. Even at large U the superfluid density is not anymore symmetric around $\rho = 0.5$ showing the absence of the particle-hole symmetry of the hard-core case. The insulating phases ($\rho_s = 0$), present at commensurate fillings for large U , start to disappear with decreasing U . Finally, for the smallest repulsive interaction we show in Fig. 15 ($U = 1$), the only insulating phase occurs at $\rho_s = 0.5$. The overall behavior is the one

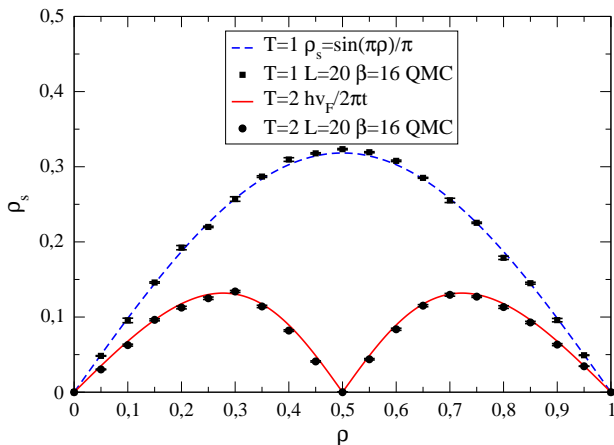


FIG. 14: (Color online) Superfluid density ρ_s as a function of density ρ . Comparison between exact analytical and numerical results at zero temperature in the thermodynamic limit, and an extrapolation using finite size and temperature QMC computations, for the uniform hard-core case, and for a case with $A = 2$ and $T = 2$.

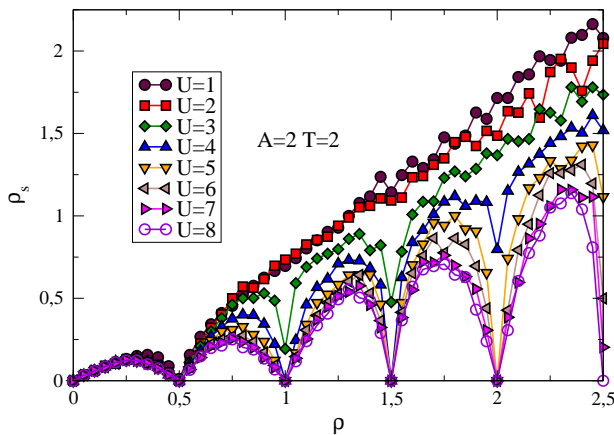


FIG. 15: (Color online) The superfluid density as a function of the density of particles, for $T = 2$, $A = 2$, and different values of the on-site repulsion U .

one would expect after Fig. 13.

As inferred from the results above, with decreasing on-site repulsion U one reaches a quantum critical point U_c for which the gap at commensurate filling vanishes, leading to a superfluid phase. This can be better seen in Fig. 16, which shows the gap as a function of U for $\rho = \frac{1}{2}$ and $\rho = 1$, and several system sizes. As U is lowered, the gap decreases but does not vanish completely if the system size is not large enough. This is due to finite size effects produced by the lattice gap. As the system size increases the lattice gap decreases and vanishes in the thermodynamic limit. Hence, in order to obtain a phase diagram one needs to do an extrapolation to check that the calculated gap does not depend on the system size.

Runs similar to those presented in Fig. 16 allowed us to obtain the phase diagram for soft-core bosons in the

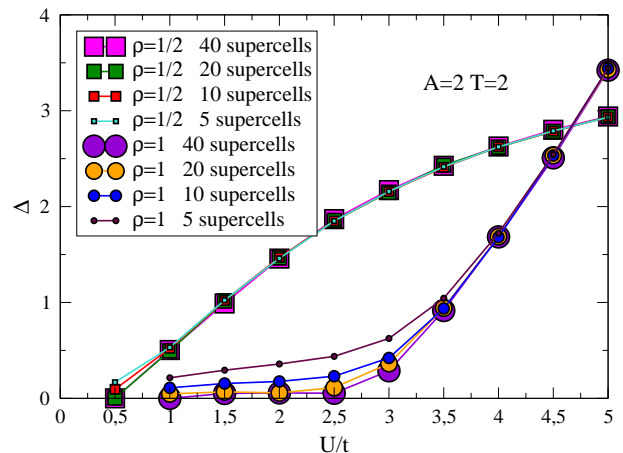


FIG. 16: (Color online) The gap as a function of U for $A = 2$, $T = 2$, $\rho = \frac{1}{2}, 1$, and several number of supercells. As the number of supercells increases, the “lattice” gap due to the finite size of the system decreases, showing evidence of a critical value of the on-site repulsion U for which the true gap vanishes.

plane μ/U vs t/U (Fig. 17). There one can see that the lobes at integer fillings are very similar to the ones of the homogeneous case depicted in Fig. 11. On the other hand, new lobes appear at $n = 1/2, 3/2, \dots$. The first extends to rather low values of U for the case $A = 2$ shown in Fig. 16.

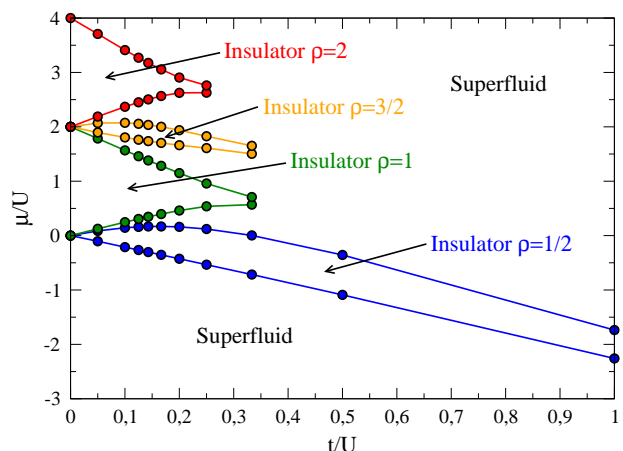


FIG. 17: (Color online) The phase diagram of soft-core bosons for $A = 2$ and $T = 2$ in the $(\mu/U, t/U)$ plane.

In order to establish a connection with the atomic limit, it is useful to draw a phase diagram in the $(\mu/U, A/U)$ plane, as in Fig. 12, for a fixed on-site repulsion $U = 8t$. This is done in Fig. 18 where we use the notations “Mott” and “CDW n ” to denote phases which have a resemblance with the ones in Fig. 12. There are some similarities with the atomic limit. For example, the region with $\rho = \frac{1}{2}$ starts with $\mu/U = 0$ for $A/U = 0$ and has a maximum value of the chemical potential close to $\mu/U = 1$ for $A/U = 1$, then goes down and crosses the

axis $\mu/U = 0$ at $A/U \approx 2$. In the region with $\rho = 1$, we have a transition from a Mott to a CDW2 at $A/U = 1$, corresponding to the critical point P_1 . The same is true for $\rho = 2$ where we have a transition from a Mott to a CDW2 at $A/U = 1$, corresponding to the critical point P_2 . The critical point P_3 is also present for $\rho = \frac{3}{2}$, and corresponds to a transition from a CDW1 to a CDW3. The main difference between the case $U = 8$ and the atomic limit $t = 0$ is that the insulating regions with commensurated fillings are separated by incommensurate superfluid regions. In addition, even the Mott insulating phases exhibit a modulation in the density, in contrast to the constant density in the usual homogeneous case. This can be seen in the plots of the structure factor (Fig. 19), which also signal clearly the transition between the different phases shown in Fig. 18.

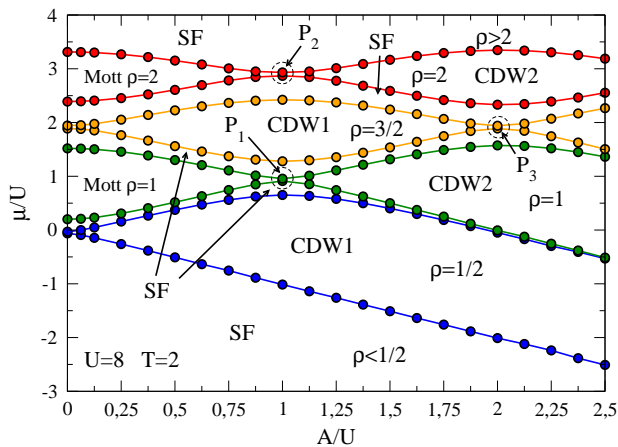


FIG. 18: (Color online) The phase diagram of soft-core bosons for $U = 8$ and $T = 2$ in the $(\mu/U, A/U)$ plane.

As U and A are decreased no extrapolation is possible from the analytical results in the hard-core and atomic limits. QMC simulations are thus essential to understand this region. At commensurated fillings we find that the competition between U and A can drive the system superfluid over a finite range of values of U and A in between Mott and CDW insulating phases. This can be seen in Fig. 20 where we have plotted the phase diagram for $\rho = 1$ and $T = 2$. Our results for intermediate values of U and A not only contrast with the atomic limit case where no intermediate phase is present, but also with studies of a similar model for fermionic systems.²⁸ We are referring to the fermionic Hubbard model with an additional $T = 2$ potential, also known as the Ionic Hubbard model. In this model an intermediate phase was also observed between the Mott insulating and band insulating phases. However, in the fermionic case the intermediate phase turned out to have a finite one particle gap²⁸ while we find it to be gapless (superfluid) in our soft-core boson case.

There are interesting qualitative and even quantitative analogies between the $T = 2$ phase diagram considered here, in which a Mott phase competes with a CDW phase

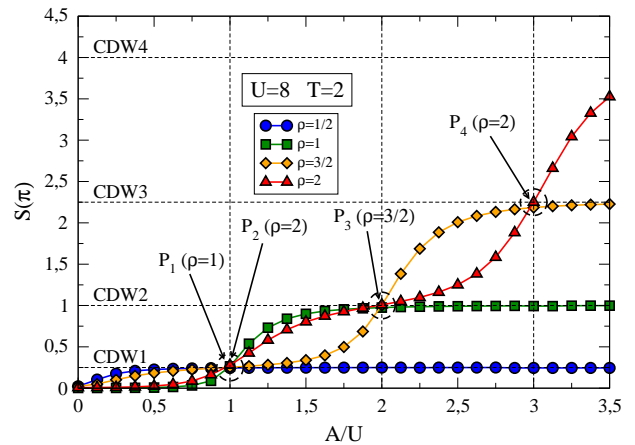


FIG. 19: (Color online) The structure factor $S(k)$ shows a peak for $k = \pi$ when the density profile is staggered. The value $S(\pi)$ allows to detect the height of the density steps. In the atomic limit, the previously defined CDW n phases correspond to $S(\pi) = \frac{n^2}{4}$. Here, in the general case, these phases are recovered when the ratio A/U is away from the critical points P_1, P_2, P_3, P_4 .

driven by the one-body superlattice potential A and the phase diagram of the extended Hubbard model where CDW correlations arise from a near neighbor interaction V .²⁹ In both cases, a superfluid region extends along a strong coupling line out to $U \approx 6t$, and the superfluid extends to arbitrarily large V or A at $U \rightarrow 0$.

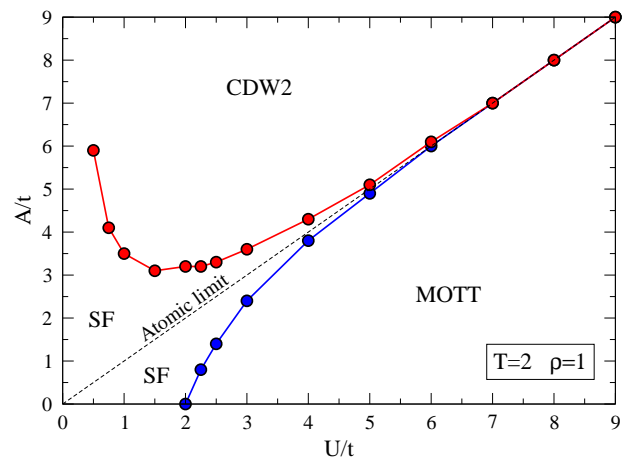


FIG. 20: (Color online) The phase diagram of soft-core bosons for $\rho = 1$ and $T = 2$ in the $(A/t, U/t)$ plane.

A behavior similar to the $T = 2$ case can be expected to hold for larger periods of the superlattice. In the appendix we present some results for the case $T = 6$ that support this conclusion.

IV. THEORETICAL ANALYSIS OF $T = 2$ MODEL

In the atomic limit ($t \rightarrow 0$), the sites are decoupled and described by atomic Hamiltonians $\hat{H}_j = (V_j - \mu) \hat{n} + U \hat{n}^2$, where $V_j = A \cos(2\pi j/T)$. As μ , A , or U is varied, there are a series of first order transitions between number eigenstates, occurring when either the particle ($\Delta_p = E(n+1) - E(n)$) or hole ($\Delta_h = E(n-1) - E(n)$) gaps collapse, where

$$\Delta_p = U(1 + 2n) + V_j - \mu \quad (14)$$

$$\Delta_h = U(1 - 2n) - V_j + \mu. \quad (15)$$

Thus, the atomic state $|K\rangle$ is the local ground state for

$$U(2n - 1) < \mu - V_j < U(2n + 1). \quad (16)$$

Note that $\Delta_p(n-1) = -\Delta_h(n)$.

Consider now the $T = 2$ case, for which $V_{2j} = +A$ and $V_{2j+1} = -A$. In the atomic limit, the eigenstates are of the form

$$|K_e, K_o\rangle = \prod_j \frac{(a_{2j}^\dagger)^{K_e} (a_{2j+1}^\dagger)^{K_o}}{\sqrt{K_e!} \sqrt{K_o!}} |0\rangle \quad (17)$$

The state $|K_e, K_o\rangle$ is the ground state provided all four gaps Δ_p^e , Δ_p^o , Δ_h^e , and Δ_h^o are positive, where

$$\Delta_{p,h}^e = U \pm (2UK_e + A - \mu) \quad (18)$$

$$\Delta_{p,h}^o = U \pm (2UK_o - A - \mu). \quad (19)$$

These four inequalities define the colored rectangular regions in Fig. 12 (see also the detail in Fig. 21.)

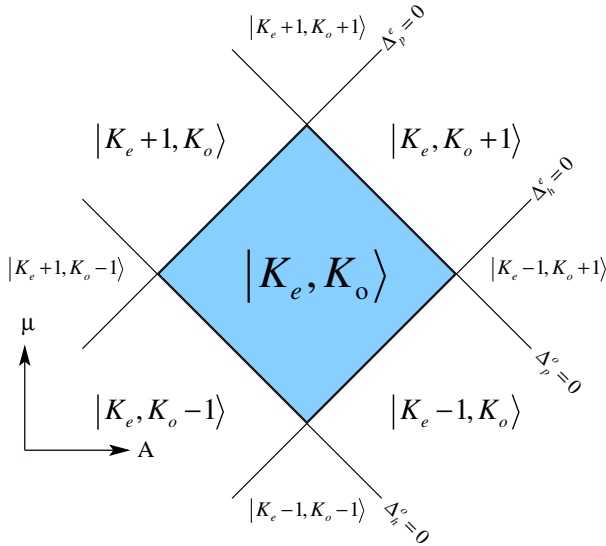


FIG. 21: (Color online) Detail of phase diagram of the $T = 2$ model in the $t = 0$ limit. The gaps are defined relative to the shaded region.

Let us now investigate the case where t/A is very small. We begin with the atomic state $|K_e, K_o\rangle$. We first assume that Δ_p^e and Δ_h^o are always positive and much larger than Δ_h^e and Δ_p^o , which puts us in the right corner of the shaded region in Fig. 21. Focusing on the lowest-lying excitations, which are holes (particles) on even (odd) sites, we arrive at the effective Hamiltonian

$$\begin{aligned} \hat{H} = & -\tilde{t} \sum_j (h_{2j}^\dagger p_{2j+1}^\dagger + h_{2j}^\dagger p_{2j-1}^\dagger + \text{H.c.}) \\ & + \sum_j (\Delta_h^e h_{2j}^\dagger h_{2j} + \Delta_p^o p_{2j+1}^\dagger p_{2j+1}) \\ & + U \sum_j (h_{2j}^\dagger h_{2j}^\dagger h_{2j} h_{2j} + p_{2j+1}^\dagger p_{2j+1}^\dagger p_{2j+1} p_{2j+1}), \end{aligned} \quad (20)$$

where h_{2j}^\dagger creates a hole (destroys a boson) on site $2j$ and p_{2j+1}^\dagger creates a particle (creates a boson) on site $2j+1$. The hopping integral is now $\tilde{t} \approx t\sqrt{K_e(K_o+1)}$. In the continuum limit, the coherent state Lagrangian density is

$$\begin{aligned} \mathcal{L} = & \bar{h} (\partial_\tau + \Delta_h) h + \bar{p} (\partial_\tau + \Delta_p) p - 2b^{-1}\tilde{t} (hp + \bar{h}\bar{p}) \\ & + \frac{1}{4} b\tilde{t} (\partial_x h \partial_x p + \partial_x \bar{h} \partial_x \bar{p}) \\ & + U(\bar{h}h)^2 + U(\bar{p}p)^2, \end{aligned} \quad (21)$$

where b is the unit cell length, and where we abbreviate $\Delta_h \equiv \Delta_h^e$ and $\Delta_p \equiv \Delta_p^o$.

Suppose $\Delta_h^e \gg \Delta_p^o$, and further assume that $U \ll t$ is very weak. Then we can integrate out the hole states in the low energy limit, obtaining the effective action

$$\begin{aligned} \mathcal{S} = & \int d\tau \left\{ \int \frac{dk}{2\pi} \left(1 - \frac{4\tilde{t}^2}{\Delta_h^2} + \frac{\tilde{t}^2 b^2 k^2}{4\Delta_h^2} \right) \bar{p}_k \partial_\tau p_k \right. \\ & \left. + \left(\Delta_p - \frac{4t^2}{\Delta_h} + \frac{\tilde{t}^2 b^2 k^2}{4\Delta_h} \right) \bar{p}_k p_k + \tilde{U} \int dx (\bar{p}p)^2 \right\}, \end{aligned} \quad (22)$$

where $\tilde{U}/U = 1 + \mathcal{O}(t^2/\Delta_h^2)$. This predicts a transition to a compressible phase when the effective p gap collapses, which occurs at

$$\Delta_p \Delta_h = \tilde{t}^2. \quad (23)$$

Alternatively, we can write a trial ground state for the model, where $\hat{h}(x)|\Psi\rangle = h|\Psi\rangle$ and $\hat{p}(x)|\Psi\rangle = p|\Psi\rangle$. The variational energy is minimized when the product ph is real, and we may then assume both p and h are real. Varying with respect to the amplitudes p and h , one obtains the coupled nonlinear equations

$$\Delta_p p + 2Up^3 - 2\tilde{t}h = 0 \quad (24)$$

$$\Delta_h h + 2Uh^3 - 2\tilde{t}p = 0. \quad (25)$$

For $\Delta_p > 0$ and $\Delta_h > 0$ and $\Delta_p \Delta_h > \tilde{t}^2$, the solution is $p = h = 0$ (i.e. a CDW state). For $\Delta_p < 0$ and $\Delta_h < 0$ and $\Delta_p \Delta_h > \tilde{t}^2$, the solution, if we assume \tilde{t} is weak, is

$p \simeq \sqrt{-\Delta_p/2U}$ and $h \simeq -\sqrt{-\Delta_h/2U}$, which is the best the coherent state description can do in approximating the neighboring CDW state $|K_e - 1, K_o + 1\rangle$. If $\Delta_p \Delta_h < t^2$ in either of these cases, the state is compressible.

If $U \gg \Delta_{p,h}^{e,o}, t$, we may assume that the number of holes or particles on each site is either zero or one, and map the problem back onto the soluble $U = \infty$ model. We stress that U does enter into the formulae for $\Delta_{p,h}^{e,o}$, so this is not entirely trivial. Again we focus on the right corner of the shaded region in Fig. 21. The $|K_e, K_o\rangle$ state is represented as $|\uparrow\downarrow\rangle$, *i.e.* a state where the ‘spin’ on each even (odd) site is polarized up (down). The effective $S = \frac{1}{2}$ Hamiltonian is then

$$\hat{\mathcal{H}} = -\tilde{t} \sum_n \left(S_n^+ S_{n+1}^- + S_n^- S_{n+1}^+ \right) + \Delta_h \sum_j S_{2j}^z - \Delta_p \sum_j S_{2j+1}^z. \quad (26)$$

Solving again via Jordan-Wigner fermionization, one has two energy bands in the reduced zone $k \in [-\frac{\pi}{2}, \frac{\pi}{2}]$ with dispersions

$$E_{\pm}(k) = \frac{1}{2}(\Delta_h - \Delta_p) \pm \frac{1}{2}\sqrt{(\Delta_h + \Delta_p)^2 + 4t^2}. \quad (27)$$

This leads to the following phase classification:

$$\Delta_h > 0, \Delta_p > 0 : \text{incompressible} \sim |\uparrow\downarrow\rangle \quad (28)$$

$$\Delta_h < 0, \Delta_p < 0 : \text{incompressible} \sim |\downarrow\uparrow\rangle \quad (29)$$

$$\Delta_h < 0, \Delta_p > 0 : |\uparrow\uparrow\rangle \text{ if } |\Delta_p \Delta_h| > t^2 \quad (30)$$

$$\Delta_h > 0, \Delta_p < 0 : |\downarrow\downarrow\rangle \text{ if } |\Delta_p \Delta_h| > t^2. \quad (31)$$

Thus, the incompressible phases occur just above and below the nodes of the phase diagram, where four atomic phases meet. This is in qualitative agreement with the numerically obtained phase diagram in Fig. 12.

V. CONCLUSIONS

The interplay between particle-particle interactions and a one body potential on the phases of correlated quantum systems is a fascinating and complicated question. In the case of a random one-body potential, the key issue is whether interactions between electrons can cause an Anderson insulator to become metallic, particularly in two dimensions, a question which has not been definitively resolved either experimentally or theoretically. The effect of interactions on a band insulator has recently been explored for the ionic Hubbard model in one dimension, with the interesting suggestion that, as in the extended Hubbard model where CDW correlations arise from interactions, there is a bond-ordered wave phase in a region where spin and charge order correlations are in a delicate balance.

This paper has provided a careful examination of the effect of correlations on boson systems in a superlattice

potential in one dimension. This is a particularly interesting case to explore, since the hard-core limit connects to the fermion problem. Indeed, as we have shown, the band insulating behavior present in the hard-core case seems to persist when U is finite, even though the bosons can now multiply-occupy the sites, and one no longer has concepts like the Pauli principle, a Fermi-surface, etc... which are key ingredients to the usual picture of a band insulator. Furthermore, we have shown that at integer fillings the transitions between insulating phases, driven by changing the ratio on-site repulsion / strength of the superlattice potential, can produce intermediate superfluid regions. This is something that could be tested in experiments with ultracold gases on optical lattices since in these intermediate regions coherence is enhanced in contrast to the insulating Mott and CDW phases.

Acknowledgments

This work was supported by NSF-DMR-0606237, NSF-DMR-0240918, and NSF-DMR-0312261. We thank C. Santana for useful input.

APPENDIX: A: LOCATOR EXPANSION FOR THE GREEN'S FUNCTION

In the $U = \infty$ case, several analytical results for the energy width of the T bands may be obtained using a locator expansion for the Green's function. For each $n \in \{0, \dots, T-1\}$, construct the quasi-momentum eigenstate $|n(k)\rangle = (T/L)^{1/2} \sum_j e^{ik(n+jT)} |n+jT\rangle$. In this basis, the Hamiltonian matrix is

$$\begin{aligned} \tilde{\mathcal{H}}_{n,n'}^k &= A \cos\left(\frac{2\pi n}{T}\right) \delta_{n,n'}^T - t e^{-i(k+\zeta)} \delta_{n',n-1}^T \\ &\quad - t e^{i(k+\zeta)} \delta_{n',n+1}^T. \end{aligned} \quad (A.1)$$

Consider a ring of T sites, which represent the consecutive states $|n(k)\rangle$. We now compute the Green's function $G(E) = (E - \hat{\mathcal{H}})^{-1}$ in this basis, using a locator expansion in powers of the hopping t . The bare ($t = 0$) Green's function is diagonal in this basis, with $G_{nn}^0 = (E - E_n^0)^{-1}$. Consider first a state which is non-degenerate in the atomic limit, *i.e.* $n = 0$ for T odd, and $n = 0$ and $n = T/2$ for T even. Let $\Sigma_{nn}^{0,\pm}$ be the self-energy contribution from all paths which start and end at n but do not contain n as an intermediate state, and which have zero net winding number (Σ^0) or wind once clockwise (Σ^-) or wind once counterclockwise (Σ^+). Summing the perturbation series for G_{nn} yields

$$G_{nn}^{-1} = (G_{nn}^0)^{-1} - \Sigma_{nn}^0 - \Sigma_{nn}^+ - \Sigma_{nn}^-. \quad (A.2)$$

The full t -dependence of the energy level $E_n(k)$ is now given by the solution to the equation

$$E = E_n^0(k) + \Sigma_{nn}^0(E) + \Sigma_{nn}^+(E) + \Sigma_{nn}^-(E), \quad (A.3)$$

which results in a pole in $G_{nn}(E)$. Since the self energy terms do not contain any factors of G_{nn}^0 , we can to a first approximation set $E = E_n^0$ therein. The self energy Σ_{nn}^0 contains infinite orders in t , but it does not accrue any phase, since it corresponds to paths of zero net winding. Therefore, it leads to a k -independent shift of the atomic energy levels. The k -dependence enters through the self energies Σ_{nn}^\pm . Since we are interested in the small t limit, we evaluate the lowest order contributions:

$$\Sigma_{nn}^+(E_n^0) = (-1)^T e^{i(k+\zeta)T} t^T \prod_{j \neq n} \frac{1}{E_n^0 - E_j^0}, \quad (\text{A.4})$$

with $\Sigma_{nn}^- = (\Sigma_{nn}^+)^*$. Thus,

$$E_n(k) = E_n^0 + \Delta E_n(t, A) - \frac{B_n t^T}{A^{T-1}} \cos(Tk + T\zeta) + \dots, \quad (\text{A.5})$$

where B_n is a constant. We now read off that the bandwidth is of order t^T/A^{T-1} .

Next consider the case of degenerate atomic levels n and $\bar{n} = T - n$. We define the self energies Σ_{nn}^0 and $\Sigma_{\bar{n}\bar{n}}^0$ as the self energy contribution from all paths starting and ending at n or \bar{n} and which contain neither n nor \bar{n} as intermediate states. We additionally define $\Sigma_{n\bar{n}}^\pm$ as the self energy contribution from all paths starting at n and ending at \bar{n} , circulating clockwise (Σ^-) or counterclockwise (Σ^+), and which contain neither n nor \bar{n} as an intermediate state. A corresponding definition holds for $\Sigma_{\bar{n}n}^\pm$, from which it follows that $\Sigma_{\bar{n}n}^\pm = (\Sigma_{n\bar{n}}^\mp)^*$. The locator expansion for $G_{nn} = G_{\bar{n}\bar{n}}$ may be summed:

$$G_{nn}^{-1} = (G_{nn}^0)^{-1} - \Sigma_{nn}^0 - \frac{|\Sigma_{n\bar{n}}^+ + \Sigma_{\bar{n}n}^-|^2}{(G_{nn}^0)^{-1} - \Sigma_{nn}^0}. \quad (\text{A.6})$$

Thus, the degenerate levels split, and are given by solutions to the equations

$$E = E_n^0(k) + \Sigma_{nn}^0(E) \pm |\Sigma_{n\bar{n}}^+(E) + \Sigma_{\bar{n}n}^-(E)|. \quad (\text{A.7})$$

Again, Σ_{nn}^0 is k -independent, and evaluating the k -dependent self energies $\Sigma_{n\bar{n}}^\pm$ to lowest order in t , we obtain (with $1 \leq n < \frac{T}{2}$),

$$\begin{aligned} \Sigma_{n\bar{n}}^+(E_n^0) + \Sigma_{\bar{n}n}^-(E_n^0) &= \frac{(-te^{i(k+\zeta)})^{T-2n}}{\prod_{j=n+1}^{T-2n-1} (E_n^0 - E_j^0)} \\ &+ \frac{(-te^{-i(k+\zeta)})^{2n}}{\prod_{j=T-n+1}^{T+n-1} (E_n^0 - E_j^0)} + \dots \\ &= C_n \frac{t^{T-2n}}{A^{T-2n-1}} e^{-i(T-2n)(k+\zeta)} \\ &+ D_n \frac{t^{2n}}{A^{2n-1}} e^{i(2n)(k+\zeta)} + \dots \end{aligned} \quad (\text{A.8})$$

$$= C_n \frac{t^{T-2n}}{A^{T-2n-1}} e^{-i(T-2n)(k+\zeta)} + \dots + D_n \frac{t^{2n}}{A^{2n-1}} e^{i(2n)(k+\zeta)} + \dots \quad (\text{A.9})$$

Thus,

$$\begin{aligned} |\Sigma_{n\bar{n}}^+(E_n^0) + \Sigma_{\bar{n}n}^-(E_n^0)| &= \frac{D_n t^{2n}}{A^{2n-1}} + \frac{C_n t^{T-2n}}{A^{T-2n-1}} \cos((T-4n)(k+\zeta)) + \dots \end{aligned} \quad (\text{A.10})$$

if $1 \leq n \leq \frac{T}{4}$, and

$$\begin{aligned} |\Sigma_{n\bar{n}}^+(E_n^0) + \Sigma_{\bar{n}n}^-(E_n^0)| &= \frac{C_n t^{T-2n}}{A^{T-2n-1}} + \frac{D_n t^{2n}}{A^{2n-1}} \cos((T-4n)(k+\zeta)) + \dots \end{aligned} \quad (\text{A.11})$$

if $\frac{T}{4} \leq n < \frac{T}{2}$. Thus the bandwidth Γ_n as well as the inverse effective mass $(m_n^*)^{-1}$ for the bands arising from the atomic levels $|n\rangle$ and $|T-n\rangle$ scales as

$$\Gamma_n \propto t \cdot \left(\frac{t}{A}\right)^{\max(2n-1, T-2n-1)}, \quad (\text{A.12})$$

where $1 < n < \frac{T}{2}$. As we shall see, this power law behavior also governs the scaling of the superfluid density with t/A in the large A limit.

Further consideration of Eq.(A.7) shows that the degenerate zero energy states at $n = p$ and $n = 3p$ for $T = 4p$ do not shift for $k = \zeta = 0$, a statement valid to all orders in t/A . The reason is that the self energy contributions Σ_{pp}^0 and $\Sigma_{p\bar{p}}^+ + \Sigma_{\bar{p}p}^-$ each vanish at $E = 0$, as a consequence of the fact that $E_{p+j}^0 = -E_{\bar{p}-j}^0$, and hence for every path contributing to these two self energy contributions there exists a path with equal and opposite amplitude, resulting in a cancellation in the locator expansion.

APPENDIX: B: $T = 6$ CASE FOR SOFT-CORE BOSONS

Figure 22 displays the density ρ as a function of the chemical potential μ for $A = 2$ and $U = 8$. As for the hard-core case, gaps appear for fractional fillings $\rho = \frac{1}{6}, \frac{2}{6}, \frac{3}{6}, \frac{4}{6}, \frac{5}{6}$. The integer fillings $\rho = 1, 2, \dots$ are also insulating, as expected from the uniform soft-core case. Again, extra gaps also appear for fractional fillings with $\rho > 1$.

The inset in Figure 22 shows the density profile for $U = 4$ and $U = 8$. As for the $T = 2$ case, the local

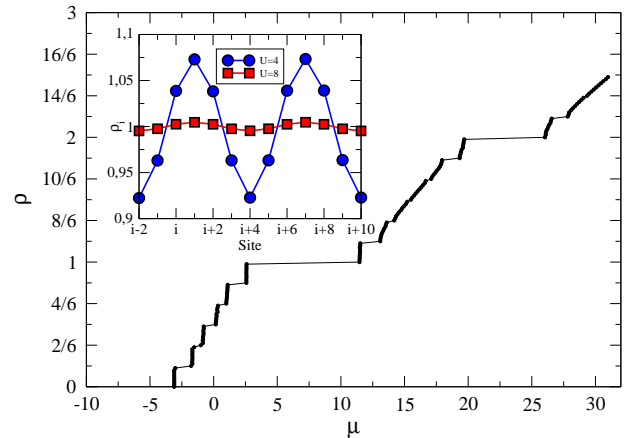


FIG. 22: (Color online) The density of particles as a function of the chemical potential for $T = 6$, $A = 2$, and $U = 8$.

density does not stick to $\rho_i = 1$. Finally, Fig. 23 shows the superfluid density which vanishes for almost each filling commensurate with the superlattice. There are some exceptions for $\rho = \frac{3}{2}, \frac{7}{3}, \frac{5}{2}$ due to the small values of the gap (see Fig. 22).

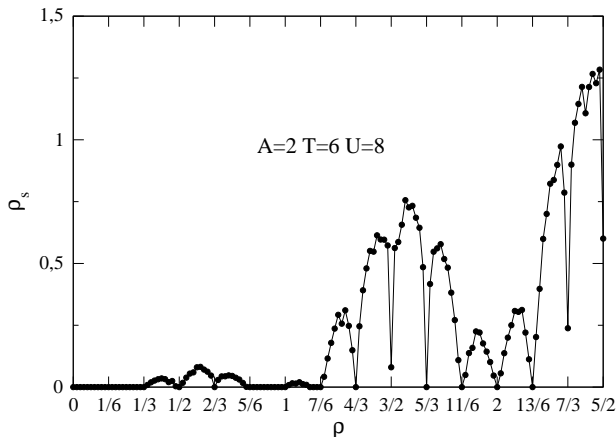


FIG. 23: The superfluid density as a function of the density of particles, for $T = 6$, $A = 2$ and $U = 8$.

-
- ¹ M.P.A. Fisher, P.B. Weichman, G. Grinstein, and D.S. Fisher, Phys. Rev. B **40**, 546 (1989).
² D. Jaksch, C. Bruder, J.I. Chirac, C.W. Gardiner, and P. Zoller, Phys. Rev. Lett. **81**, 3108 (1998).
³ G.G. Batrouni, R.T. Scalettar, and G.T. Zimanyi, Phys. Rev. Lett. **65**, 1765 (1990).
⁴ T.D. Kuhner, S.R. White, and H. Monien, Phys. Rev. B **61**, 12474 (2000).
⁵ J. K. Freericks and H. Monien, Phys. Rev. B **53**, 2691 (1996).
⁶ W. Krauth and N. Trivedi, Europhys. Lett. **14**, 627 (1991).
⁷ A. van Otterlo and K.H. Wagenblast, Phys. Rev. Lett. **72**, 3598 (1994).
⁸ For studies of a closely related current model, see A. Kuklov, N. Prokof'ev, and B. Svistunov Phys. Rev. Lett. **93**, 230402 (2004), and references cited therein.
⁹ R.T. Scalettar, G.G. Batrouni, and G.T. Zimanyi, Phys. Rev. Lett. **66**, 3144 (1991).
¹⁰ W. Krauth, N. Trivedi and D. Ceperley, Phys. Rev. Lett. **67**, 2307 (1991). K.G. Singh and D.S. Rokhsar, Phys. Rev. B **46**, 3002 (1992). E.S. Sorensen, M. Wallin, S.M. Girvin, and A.P. Young, Phys. Rev. Lett. **69**, 828 (1992). K.J. Runge, Phys. Rev. **45**, 13136 (1992).
¹¹ G.G. Batrouni, V.G. Rousseau, R.T. Scalettar, M. Rigol, A. Muramatsu, P.J.H. Denteneer, and M. Troyer, Phys. Rev. Lett. **89**, 117203 (2002).
¹² S. Wessel, F. Alet, M. Troyer, and G.G. Batrouni, Phys. Rev. A **70**, 053615 (2004).
¹³ P. Buonsante and A. Vezzani, Phys. Rev. A **70**, 033608 (2004).
¹⁴ P. Buonsante, V. Penna, and A. Vezzani, Phys. Rev. A **70**, 061603 (2004).
¹⁵ P. Buonsante, A. Vezzani, Phys. Rev. A **72**, 013614 (2005).
¹⁶ J.B. Sokoloff, Phys. Rep. **126**, 189 (1985).
¹⁷ Y. Last, Proc. of XIth Int. Congress of Math. Phys. 366, 1994; S. Jitomirskaya, *ibid*, 373.
¹⁸ V.W. Scarola and S. Das Sarma, cond-mat/0506415.
¹⁹ N.R. Thomas, C.J. Foot, and A.C. Wilson, cond-mat 0108169.
²⁰ S. Friebe, C.D'Andrea, J. Walz, M. Weitz, and T.W. Hansch, Phys. Rev. A **57**, R20 (1998).
²¹ P. Ahmadi, V. Ramareddy, and G.S. Summy, New J. Phys. **7**, 4 (2005).
²² S. Peil, J.V. Porto, B. Laburthe Tolra, J.M. Obrecht, B.E. King, M. Subottin, S.L. Rolston, and W.D. Phillips, Phys. Rev. A **67**, 051603(R) (2003).
²³ M. Rigol and A. Muramatsu, Phys. Rev. A **70**, 031603(R) (2004); **72**, 013604 (2005).
²⁴ V.G. Rousseau, R.T. Scalettar, and G.G. Batrouni, Phys. Rev. B **72**, 054524 (2005).
²⁵ G. G. Batrouni and R. T. Scalettar, Phys. Rev. B **46**, 9051 (1992).
²⁶ M. A. Cazalilla, Phys. Rev. A **67**, 053606 (2003).
²⁷ E.L. Pollock and D.M. Ceperley, Phys. Rev. B **36**, 8343 (1987).
²⁸ S.R. Manmana, V. Meden, R.M. Noack, K. Schönhammer, Phys. Rev. B **70**, 155115 (2004), and references cited therein.
²⁹ P. Niyaz, R.T. Scalettar, C.Y. Fong, and G.G. Batrouni, Phys. Rev. B **44**, 7143 (1991); **50**, 362 (1994).
³⁰ J. Sebby-Strabley, M. Anderlini, P. S. Jessen, and J. V. Porto, cond-mat/0602103 [Phys. Rev. A (to be published)].